Negative Piezoresistive Effect in a Stretchable Device Based on a Soft Tunneling Barrier

Soosang Chae (chae@ipfdd.de)
Leibniz-Institut für Polymerforschung Dresden e. V.
Ivan Fotev
Helmholtz-Zentrum Dresden-Rossendorf
Eva Bittrich
Leibniz-Institut für Polymerforschung Dresden e. V.
Won Jin Choi
University of Michigan - Ann Arbor https://orcid.org/0000-0001-6303-8899
Petra Uhlmann
Leibniz-Institut für Polymerforschung Dresden
Mathias Schubert
University of Nebraska-Lincoln
Alexej Pashkin
Helmholtz-Zentrum Dresden-Rossendorf https://orcid.org/0000-0003-1309-6171
Andreas Fery (fery@ipfdd.de)
Leibniz Institute of Polymer Research

Article

Keywords: negative piezoresistive material, tunable quantum barrier, quantum scale thinning, near-zero standby power consumption, soft and stretchable electrode

Posted Date: October 30th, 2020

DOI: https://doi.org/10.21203/rs.3.rs-99307/v1

Negative Piezoresistive Effect in a Stretchable Device Based on a Soft Tunneling Barrier

Soosang Chae[1], Ivan Fotev[2,3], Eva Bittrich[1], Won Jin Choi[4], Petra Uhlmann[1,5], Mathias Schubert,[1,6,7] Alexej Pashkin[2], Andreas Fery[1,3*]*

[1]Leibniz-Institut für Polymerforschung Dresden e.V, Hohe Straße 6, 01069 Dresden, Germany

[2]Institute of Ion Beam Physics and Materials Research, Helmholtz-Zentrum Dresden-Rossendorf, 01328 Dresden, Germany

[3]Technische Universität Dresden, 01062 Dresden, Germany

[4]Departement of Materials Science and Engineering, University of Michigan, Ann Arbor, MI, USA

[5]Department of Chemistry, University of Nebraska-Lincoln, Lincoln, Nebraska 68588, USA

[6]Department of Electrical and Computer Engineering, University of Nebraska-Lincoln, Lincoln, Nebraska 68588, USA

[7]Department of Physics, Chemistry and Biology, (IFM), Linkoping University, 58183 Linkoping, Sweden

* email : chae@ipfdd.de (Dr. S. Chae), fery@ipfdd.de (Prof. A. Fery)

Abstract

Piezoresistive soft composite materials are widely used in strain sensing and typically exhibit a decrease in conductivity upon elongation—the so-called positive gauge effect. We demonstrate a thin-film architecture that features the inverse behavior: a strain-induced transition from insulating to metallic conductivity, spanning nine orders of magnitude in conductivity. Our approach is based on a nanometer-scale sandwiched bilayer Au thin film with a polydimethylsiloxane elastomeric barrier layer. Upon application of strain, the thickness of the thin soft barrier decreases because of the strain governed by the Poisson effect, followed by electron-tunneling currents through the barrier, forming an interconnected bilayer metal electrode. An extremely high on–off electrical conductivity ratio (~10^9) is observed over a wide range of working strains (as high as 130%), which mimics the ideal features of a mechanical-force-controlled electric transistor. This conceptual design strategy is expected to benefit a wide range of applications in which operation under minimal standby power could be an essential feature, such as in implantable soft strain sensors and in prosthetic long-term monitoring systems for detecting sudden a swelling/volume expansion of human body organs or blood vessels, thereby helping to avoid acute and severe syndromes.

Keywords

negative piezoresistive material, tunable quantum barrier, quantum scale thinning, near-zero standby power consumption, soft and stretchable electrode

Introduction

State-of-the-art strategies to achieve flexible and stretchable sensor devices, which are strongly demanded for diverse applications such as flexible and highly deformable electronics and devices,[1,2] artificial skin,[3,4,5] implantable health monitoring sensors,[6,7] and soft actuators/robotics,[8,9] mostly rely on forming and breaking a percolated network of a conductive filler and thus always resulting in an increase in resistance under stretching.[10] However, for power-conserving applications in a long-term standby strain sensor,[11] a negative gauge factor (nGF) is desirable, where, in the off-mode, a large resistance with $R_0 \cong \infty$ ensures low power consumption and a potentially long operating lifetime and where a small on-mode resistance under strain ($R_\varepsilon \ll R_0$) enables reliable detection. Near-zero power consumption ($P = I \cdot V \cong 0$) is important, for example, in implantable nanodevices and prosthetic monitoring systems.

Negative piezoresistivity has rarely been observed in condensed matter such as metals (e.g., Ni) and semiconductors (e.g., *n*-type Si, Si nanowires, and some two-dimensional semiconductors).[12,13,14,15] Practical applications of negative piezoresistivity in soft/stretchable devices is further limited by their high Young's modulus and extremely low maximum yield strength.[13,14,15] The fabrication of composite stretchable negative-piezoresistive materials by, for example, utilizing a negative-piezoresistive filler embedded in an elastic matrix has been suggested.[16,17,18] However, the increased interspacing of the filler upon application of strain within a certain range counteracts the resistance reduction of the composite and the nGF strain range is limited to extremely small strain variations (ε = ~%).[16,17] The low off-mode resistance is not favorable for low power consumption in the standby mode. In addition, the resistance modulation in the on-state (with strain) is limited by the elastic matrix of the surrounding insulator; therefore the performance of stretchable composite materials with

negative piezoresistivity is hampered by a poor on-to-off ratio (10^2 - 10^3) and a low operating nGF strain range.

One of the fascinating properties of soft and elastomeric materials is that, if elastomers are used as a tunneling barrier material between two electric terminals, the potential barrier can be tuned *via* quantum-scale thinning by macroscopic stimulation, *i.e.*, by mechanical strain, analogous to the gate effect in transistors. The ability to achieve current modulation across many orders of magnitude and the fact that one key parameter is a mechanical property (*i.e.*, a thickness related to barrier height controlled by strain) together promise untapped possibilities for a new strategy toward stretchable piezoresistive materials with negative piezoresistivity.

Here, we report a new design of a stretchable negative piezoresistive device using a bilayer metal thin film sandwiching an ultrathin soft insulator barrier layer. Upon application of strain, the conductivity between the electrically contacted bilayer metal thin film undergoes a superior transition from $\sigma_{\varepsilon=0} \approx 10^{-5}\,\Omega^{-1}\mathrm{cm}^{-1}$ at zero strain to $\sigma_{\varepsilon=1.0} \approx 10^{5}\,\Omega^{-1}\mathrm{cm}^{-1}$ at unity strain. The very high off-state resistivity, the wide working range of negative piezoresistive strain, and the high conductivity in the on-state exceed the properties of all known stretchable conductors[19–25] and negative piezoresistive materials.[10] To illustrate the versatility and applicability of this new negative piezoresistivity concept, we demonstrate a mechano-gated stretchable electrical switch device and a zero-standby-power strain sensor. This work paves the way toward numerous stretchable-strain-sensor applications that rely on long-term standby-mode strain monitoring with minimal power consumption.

Design of the sandwiched bilayer metal thin film with a soft thin barrier layer

To achieve stretchable negative piezoresistivity, a material must exhibit not only superior stretchable conductivity in the highly stretched state but also insulating behavior in its initial state; thus, a key challenge is developing new materials whose conductivity rapidly increases upon application of mechanical strain. We started our work by depositing a metal thin film onto an elastomer substrate via the physical vapor deposition (PVD) method. The relatively brittle metal thin film readily formed many cracks and lost its electrical interconnectivity once the underlying elastomer substrate was stretched; the metal thin film deposited onto the elastomer substrate showed a positive gauge factor (pGF) ($R_\varepsilon \gg R_0$) (Supplementary Fig. 1 and scheme in Fig. 1c). Our new proposed design is composed of bilayer metal thin films with a thin soft intermediate layer placed between the metal layers as an insulating tunnel barrier. The layers are sequentially stacked on the substrate (see details in Methods and Supplementary Information S1 and Supplementary Fig. 2). The structural properties of the bimetal and soft-barrier thin-film device are shown in a cross-section dark-field scanning transmission electron microscopy (STEM) image (Fig. 1a) and in elemental line profiles of Si and Au core emissions obtained by energy-dispersive X-ray spectroscopy (EDS) (Fig. 1b). As discussed in the next section, the thin soft elastomeric barrier layer decreases in thickness because of the *Poisson* effect, which is expected to affect the interconnectivity between the metal bilayers upon the application of external strain. The PVD method enabled precise control of the thickness of the metal bilayers, which allowed us to exploit the percolation threshold at which the transition from the conductive to the nonconductive state of a thin metal layer occurs. Hence, by optimizing the deposition thickness (percolation engineering) and by controlling the deposition conditions of the soft tunneling barrier layer, we systematically obtained a stretchable electrode possessing all three modes of a stretchable gauge factor: positive, zero, and negative (Fig. 1c–e). In particular, such an optimized design enables, for the first time, the fabrication of a high-performance negative-piezoresistive

stretchable device and can provide an excellent platform for developing multimode piezoresistive strain sensors suitable for applications that require responsiveness to a wide range of strain in a single system.

Mechanism of nGF: Percolation engineering and quantum thinning

To study the effect of metal-layer thickness on the nGF property, the resistivity change at applied strains ($0 \leq \varepsilon \leq 0.31$) was plotted for various deposition thicknesses of both layers (the first metal layer, $d_{1\mathrm{st}}$, and the second metal layer, $d_{2\mathrm{nd}}$) as a contour plot in Fig. 2a. We categorized the deposition thicknesses into three classes according to the different tendencies observed: "A" ($d_{1\mathrm{st}} < 25$ nm, $d_{2\mathrm{nd}} < 17.5$ nm), "B" ($d_{1\mathrm{st}} > 32.5$ nm, $d_{2\mathrm{nd}} > 25$ nm), and "C" (25 nm $< d_{1\mathrm{st}} < 32.5$ nm, 17.5 nm $< d_{2\mathrm{nd}} < 25$ nm). The corresponding resistivity changes for the full range of strain ($0 < \varepsilon < 1.0$) and the change rate, $\frac{\mathrm{d}(\log\rho)}{\mathrm{d}\varepsilon}$, are shown in Fig. 2b–d. Note that only region C shows the nGF property, $\rho_{\varepsilon=0} > 10^{12}, \rho_{\varepsilon=0.06} \approx 10^{10}, \rho_{\varepsilon=0.12} \approx 10^{7}, \rho_{\varepsilon=0.18} \approx 10^{5}$, and $\rho_{\varepsilon=0.31} < 10^{4}\ \Omega \cdot \mathrm{cm}$, whereas the others maintain a constant resistivity either greater than $10^{12}\ \Omega \cdot \mathrm{cm}$ (region A) or less than $10^{3}\ \Omega \cdot \mathrm{cm}$ (region B) for any applied strain. Indeed, region C well matched the percolation threshold thickness for each metal layer (Supplementary Fig. 3). Interestingly, the constant resistivity ($< 10^{3}\ \Omega \cdot \mathrm{cm}$ to $\varepsilon = 100\ \%$) observed for region B represents superior electrical stretchability compared with that of the control sample (Supplementary Fig. 4), which implies that the structure is not only useful for attaining a high nGF but is also suitable for use in a wide range of soft electronic applications. For example, with a simple variation in the thickness of the metal layers, the resultant zero Gauge Factor (zGF) property could make the structure applicable as a stretchable interconnector with stable and superior stretchable conductivity (also utilized in the following demonstration subsection). As a result of the optimization of the deposition thickness (percolation engineering as scheme in

Supplementary Figs. 5 and 6), the structure is electrically isolated at the beginning as a consequence of the intraconduction path being disallowed because of the insufficient deposition thickness and because the soft barrier layer with a proper high potential barrier is sufficient to prevent a tunneling current between the metal layers (Fig. 3a). Upon the application of strain, the thickness of the barrier layer begins to decrease, whereas its length increases along the strain direction. Although the gaps between the intrametal domains in both layers may also increase, the thinning is expected to lead to a tunneling current across them.

We have conducted Terahertz time-domain spectroscopy (THz-TDS) measurements on a stretched polydimethylsiloxane (PDMS) sample to evaluate the thinning. The normalized average value shown in Fig. 3e (red line) shows the PDMS thickness as a function of strain. It was measured at two positions: in the center of the PDMS substrate and halfway off-center (Supplementary Fig. 7). Notably, the results are comparable to the computational simulation results obtained using the finite element method (Fig. 3d, Supplementary Information S2, and Supplementary Fig. 8). Knowing the thickness variation of the PDMS layer under strain, we can model the conductance of the structure using the tunneling model proposed by Simmons.[26] In the limit of low voltages V, when the potential drop across the barrier is much smaller than the average barrier height ($eV << \varphi$), the tunneling current should be directly proportional to V. This condition indeed holds for the studied PDMS sample, as evidenced by the current–voltage (I–V) curves recorded for different strains. All of the I–V curves are approximately linear (R^2 in inset) over the whole applied strain range ($\varepsilon = 0 \rightarrow 1$) (Fig. 3f). Note the different current scales for different applied strains. Therefore, the generalized equation for the tunneling current can be simplified to[27]

$$j = \frac{\sqrt{2m\varphi}}{s(\varepsilon)}\left(\frac{e}{h}\right)^2 V\, exp\left[-\frac{4\pi s(\varepsilon)}{h}\sqrt{2m\varphi}\right], \quad (1)$$

where $s(\varepsilon)$ is the barrier thickness dependent on strain ε and m is the electron mass. We assume that, for moderate strains ($\varepsilon < 0.5$), the thin PDMS layer is bonded to the substrate and that its change in relative thickness follows the substrate deformation characterized by the TDS-THz measurements. The initial thickness (without strain) was set to 12 nm; this value was measured by ellipsometry on a model sample on a Si-wafer substrate (see details in Supplementary Information S3 and Supplementary Fig. 9). The calculated conductance of the nGF device is shown in Fig. 3e together with the measured values. The barrier height was set to φ= 2.3 eV to achieve the best agreement with the experimental data. Obviously, for $\varepsilon >$ 0.5, the conductance saturates and does not demonstrate the model's prediction of exponential growth with increasing strain. We speculate that, at such large strain, the thin PDMS barrier layer begins to slip and loses its bonding with the substrate. As a result, the barrier thickness does not vary as the applied strain is increased further, leading to the observed current saturation. Presumably, the lateral conductivity (*via* intraconduction) also must change at such large strain regions. For other future material configurations, as evident from Fig. 3g, both the initial thickness of the barrier layer (s_0) and the barrier height (φ) between the metal/barrier interface jointly determine the negative gauge factor: larger nGF values are expected for thicker and higher barriers. However, an excessively thick barrier in either height or initial thickness could give rise to a huge resistivity, which implies a certain limitation to the expected nGF value for this design.

High performance of negative piezoresistive and demonstration of a zero-power strain sensor

We compared the electromechanical performance of our device with those of state-of-the art, stretchable piezoresistive composites. Although stretchable piezoresistive composite materials have been widely developed for various working strains with a wide range of GF

values, the GF values are all positive (Fig. 4a). Hence, inevitably, all stretchable devices have a finite resistance in the absence of strain and are not suitable for low-power standby strain sensor applications. By contrast, the GF of our nGF piezoresistive elastomer shows an average nGF of −14.5, which is comparable to the previously reported values; however, these previously reported values have only been reported in a small number of papers.[16,17] Notably, the negative piezoresistive range of our sample extends to 130% strain, and no pGF features are observed at any applied strain.

We also compared the strain-dependent absolute DC conductivity of our nGF piezoresistive device (Fig. 4b,c), which can be the most important characteristic for realizing a zero-standby-power strain sensor via low current flow in the standby mode. When the electrode is in the "off" state (i.e., in the absence of strain), the initial conductivity of our device is almost outside the measurable range ($\sigma_{\varepsilon=0} = 10^{-5}\ \Omega^{-1}\mathrm{cm}^{-1}$); when the electrode is in the "on" state (in this case, $\varepsilon > 50\%$), the conductivity even exceeds the performance of other stretchable electrodes reported elsewhere.[19–25] Electrical conduction in our structure in the stretched state can occur between two pure metal thin films without any interruption from the insulating matrix, resulting in superior on-state conductivity ($\sigma_{\varepsilon=1.0} = 10^{5}\ \Omega^{-1}\mathrm{cm}^{-1}$) comparable to the conductivity of pristine bulk metals (e.g., Ag and Au, $> 10^{6}\ \Omega^{-1}\mathrm{cm}^{-1}$). Note that this value is superior to any other reported value of stretchable electrodes in both of electrical conductivity and stretchability. As a straightforward demonstration, we visualized the pGF, zGF, and nGF performances with three of our selected devices (Fig. 5). Their high-resistivity switching dynamic with the corresponding *I–V* curves was revealed by either fully conducting the current necessary to operate a light-emitting diode (LED) irrespective of strain (zGF), at zero strain while blocking the LED current at nonzero strain (pGF), or at nonzero strain while blocking the LED current at zero strain (nGF) (bottom of Fig. 5 and

Supplementary Movie 1).

The strain for the transition tendency of the nGF resistivity can be modulated by varying the initial thickness of the PDMS soft barrier layer (Fig. 6c and Supplementary Information S4), which is potentially advantageous for extending the range of applications to include widely varying scenarios that require different threshold strains. The resistivity response of the nGF strain sensor to a stepwise increment of applied strain is shown in Fig. 6e. The excellent operational stability and reliability was demonstrated with different strains of ε = 0.015 and ε = 0.05 steps at different time intervals of 60 s and 25 s, respectively. We conducted a few cycle tests by repeating the application and release of strain at ε = 0.1. The on-to-off ratio was constant from the first to the final cycle, which revealed reproducible and reliable strain detection (Fig. 6d and Supplementary Fig. 10).

To demonstrate the potential applications of the nGF behavior, on the basis of the results in Fig. 2, we fabricated a stretchable strain sensor by incorporating both the zGF (for a stretchable interconnector) and nGF (for the area of the sensing grid) features on a single device (a digital image of the as-fabricated device in Fig. 6a,b is shown in Supplementary Fig. 11). The extremely high resistivity in the sensing-grid region contributed to an almost zero current draft across the whole circuit, which means that power consumption in standby mode in the absence of strain was reduced (Supplementary Fig. 12). This power-saving ability of the nGF piezoresistive elastomer makes the sensor highly suitable as a long-term strain monitor on massive infrastructure (Fig. 6f and Supplementary Fig. 13). In comparison to a normal strain sensor (HBM, 1-LY11-6) that shows a constant current flow of ~1.2 mA in standby mode (see brown line in top of Fig. 6g), the nGF strain sensor showed no current flow (~0 mA; black line in top of Fig. 6g). Thus, the accumulated power consumption was maintained at almost zero in the standby mode (black line in bottom of Fig. 6g). If the

duration of the standby mode becomes longstanding (~ years), these differences will be even more prominent. Thus, this lightweight and morphable nGF strain sensor could be very effectively implemented in long-term standby mode to detect early signs of collapse and sudden change in the systems spanning from organs in body to massive structures due to earthquakes.

In conclusion, the bilayer metal thin film with an intermediate thin soft insulator layer on a stretchable substrate enables a dramatic transition in conductivity under applied mechanical strain. Starting from insulator-like conductivity (10^{-5} S cm^{-1}), it exhibits an extremely high on/off ratio (~10^{9}) and metal-like conductivity (10^{4} S cm^{-1}) is achieved for strain as high as 130% in the piezoresistive device. Theoretical modeling was conducted with the low-voltage limited Simmons' tunneling equation to elucidate the working mechanism in this structure. The extremely high nGF property with a wide working range of applied strains opens the possibility of zero-standby-power strain sensors for buildings or health monitoring, and can be particularly suitable to identify unexpected organ expansion in the human body, with a long device lifetime.

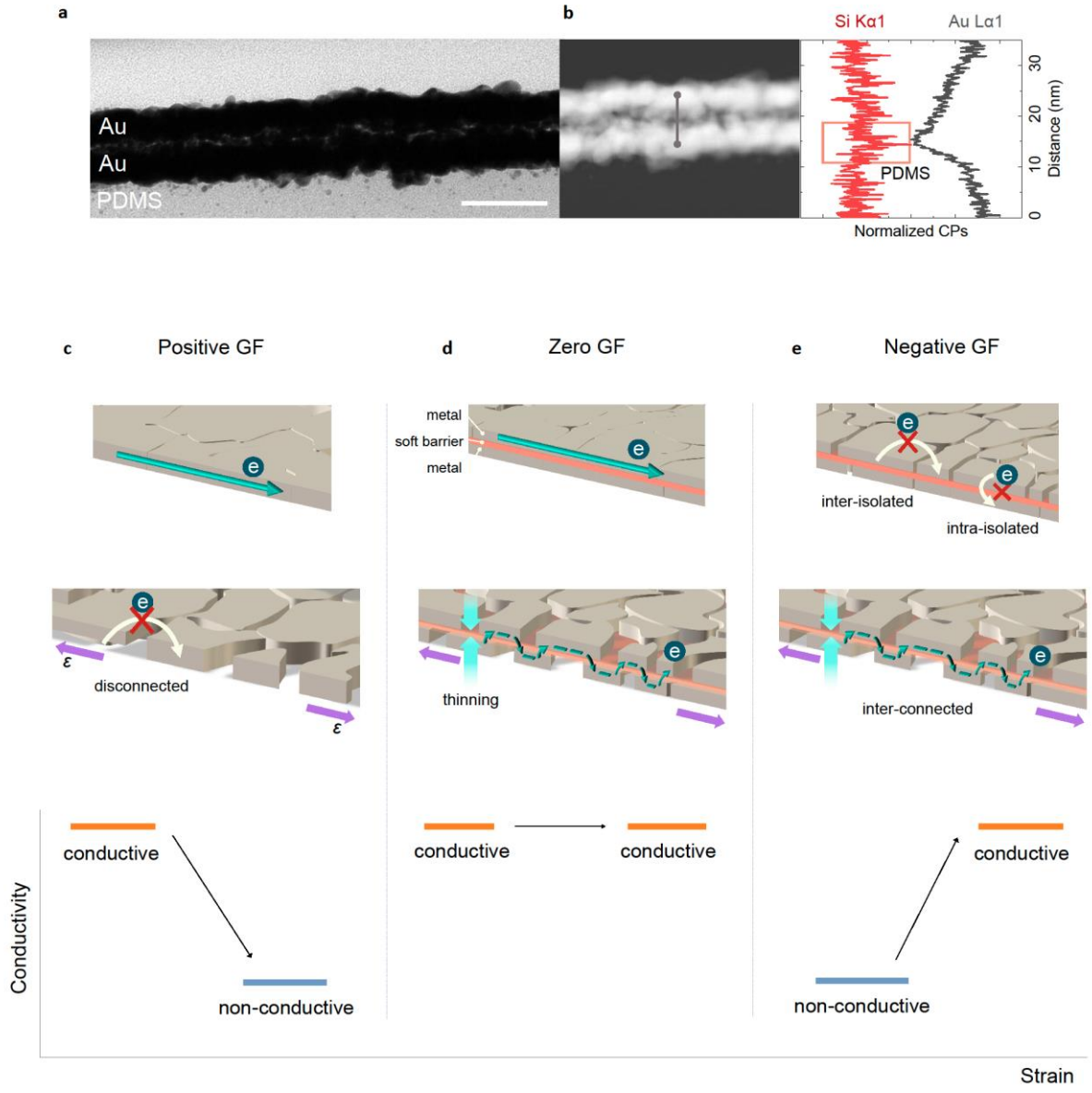

Figure 1. Sandwiched bilayer metal thin film with a soft barrier layer for all types of piezoresistive stretchable electrodes. a, nGF stretchable piezoresistive device with a bimetal layer (each 20–30 nm thick) and thin soft insulator barrier layer (~12 nm thick); scale bar, 100 nm. **b,** Scanning TEM image of the device with line profile of the energy-dispersive X-ray spectra of Si and Au atoms for identifying the soft barrier layer (e.g., PDMS) sandwiched in the metal thin-film bilayer (e.g., Au). **c,d,e,** With precise control of the deposition thickness of the bimetal thin film (e.g., percolation engineering) and quantum-scale thinning of the soft barrier layer upon stretching, the designed structure shows all three modes of GF (**c**, pGF; **d**, zGF; **e**, nGF). In particular, for the nGF property, an extremely high on/off electrical

conductivity ratio was obtained over a wide range of working strains.

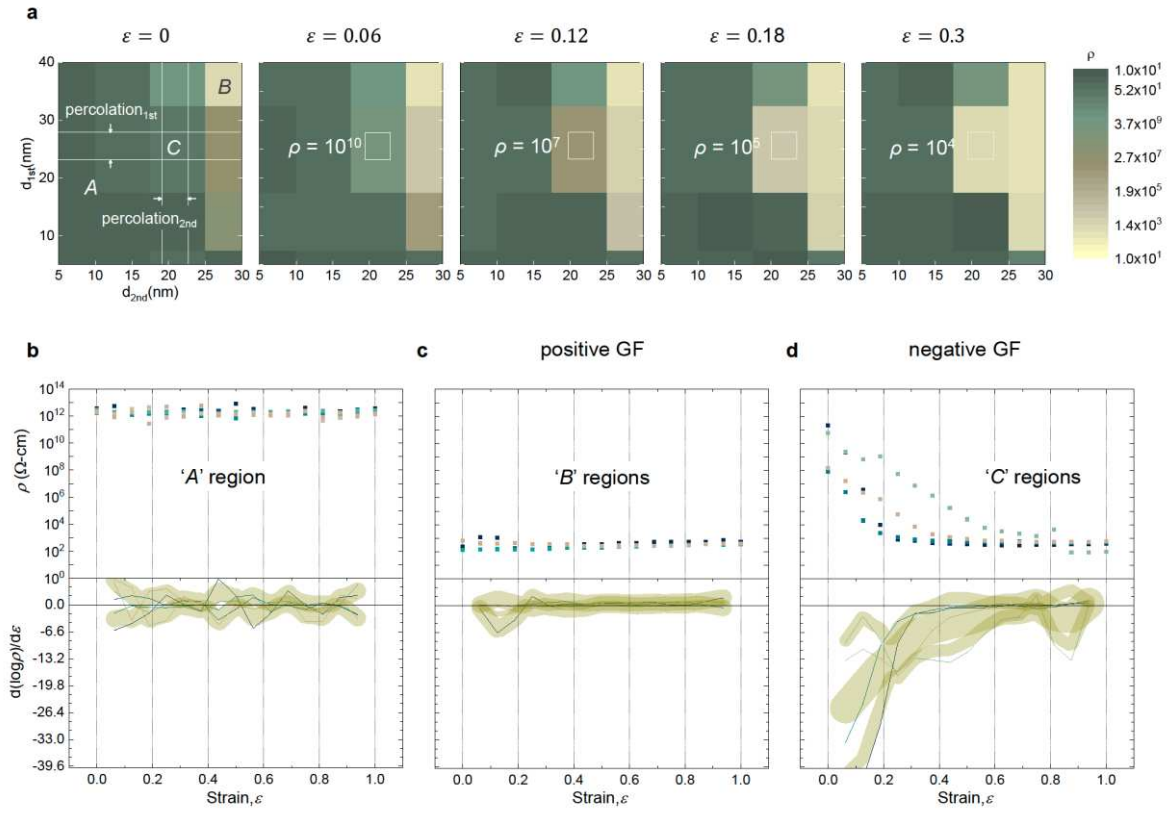

Figure 2. Thickness effect of the metal layer on nGF behavior. a, The nGF behavior is dependent on the thickness of the bimetal layer. For different combinations of the two layer thicknesses (vertical axis: first layer; horizontal axis: second layer), the change tendency of resistivity in the bilayer electrode with various strains (ε = 0, 0.06, 0.12, 0.18, 0.3) was classified as constant insulator-like ("A" combination), constant metal-like conduction ("B" combination), and transition from insulator-like to a metal-like conduction, nGF ("C" combination), where the percolation thickness of each metal layer is the criterion for determining the classification (see Supplementary Fig. 5). **b,c,d,** The resistivity change of respective regions in the full range of applied strain ($\varepsilon = 0 \rightarrow 1$) and the corresponding rate of change for the "A" combination (**b**), "B" combination (**c**), and "C" combination (**d**). A stretchable device satisfying combination "C" shows only the dramatic transition in resistivity under applied strain, i.e., high nGF performance.

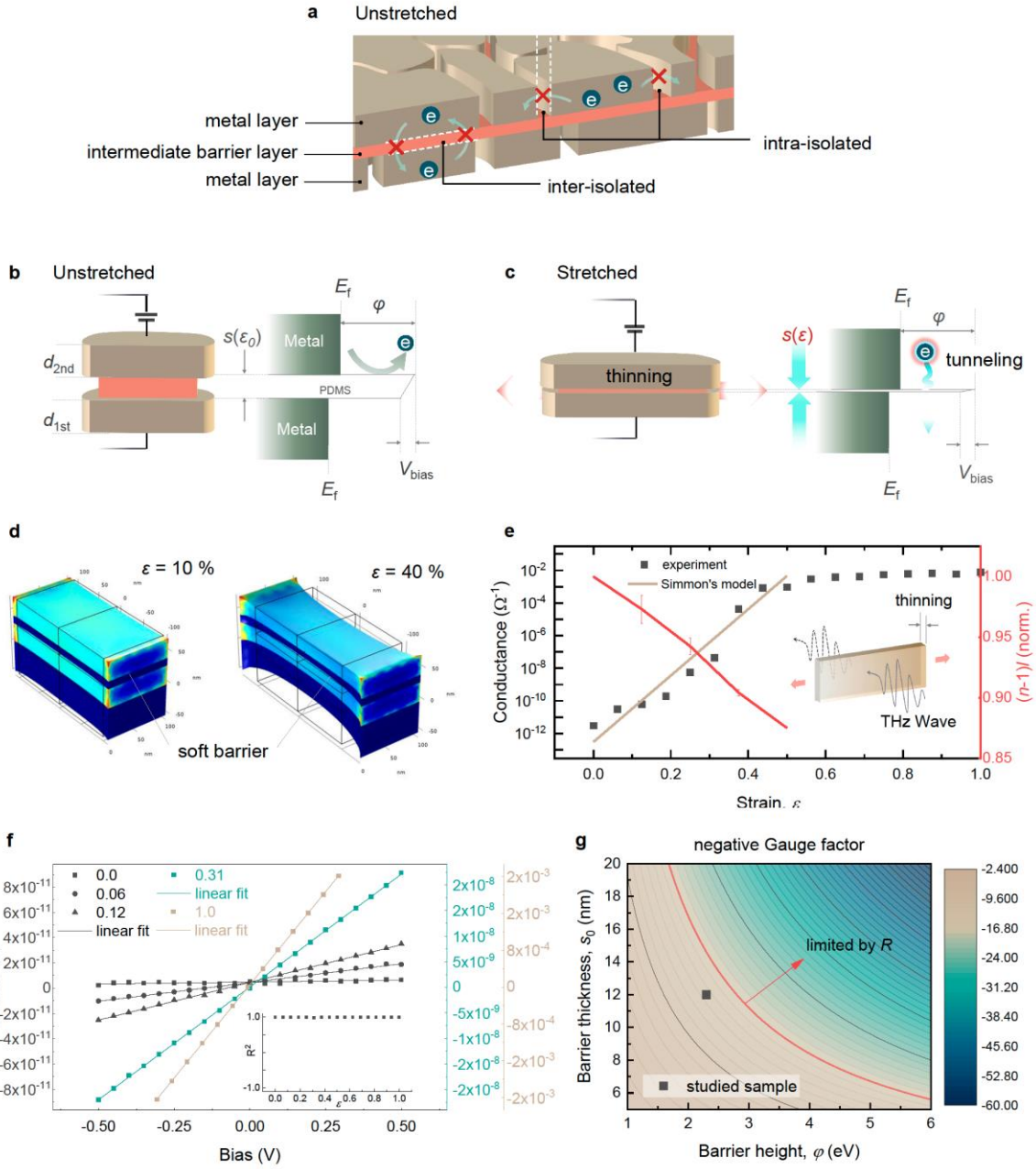

Figure 3. Working principle of the nGF piezoresistive device: tunneling current caused by thinning of the soft barrier layer. a, Schematic of the nGF piezoresistive device in its initial state (without stretching), where two metal layers are electrically not only intra-isolated via controlled percolation but also interisolated by an inserted thin soft intermediate insulating layer. **b,c,** Energy-level diagrams of an nGF stretchable electrode in the unstretched (**b**) and stretched (**c**) states, where electrons transport through the thinned barrier layer caused by stretching (s_ε), whereas no electron transport occurs because of the sufficient thickness ($s_{\varepsilon 0}$) with a high barrier height (φ) without stretching. **d,** Theoretical thinning of the

soft barrier layer simulated by the finite element method (Supplementary Fig. 7). **e,** Strain-dependent conductance with experimentally measured thinning of the soft barrier layer, as measured by THz-TDS (red line). Measured conductance of an nGF stretchable electrode sample (black dots) and the calculation according to low-voltage limited Simmons' tunneling equation, Eq. (1) (brown line). **f,** *I–V* curves of an nGF stretchable device at different applied strains; all of the curves show linear behavior independent of the applied strain. Note that the current scales differ for different applied strains (inset: R^2 of the linear fit in the strain range from 0.0 to 1.0). **g,** Expected nGF as a function of the variation in the potential barrier height and the initial thickness of the soft barrier layer. Solid black squares (e.g., nGF = −14.8) indicate the nGF value for the sample studied in this work. Note that, beyond the red boundary line, the nGF value could be limited in practical applications because of excessively high resistance. Each line corresponds to an nGF level from −5 to −50 with a step of 10.

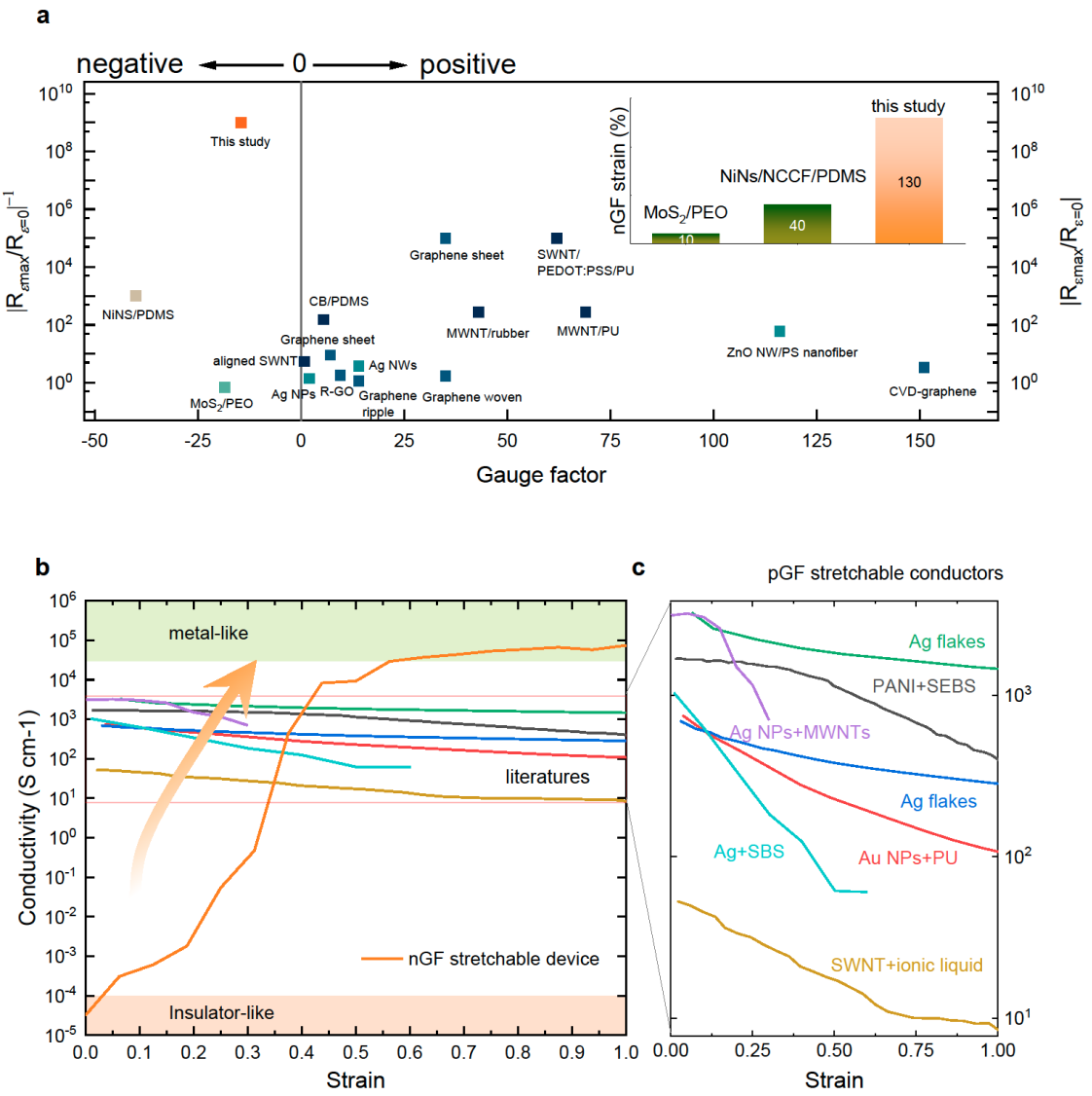

Figure 4. High performance of the nGF piezoresistive stretchable structure. a, The performance of the bilayer metal nGF stretchable electrode is compared with that of state-of-the-art stretchable piezoresistive materials. The maximum nGF strain range (to 130%) of the bilayer metal stretchable electrode represents the best-available stretchability among the developed negative piezoresistive materials (inset). **b,** Measured DC conductivity with respect to applied strain of the nGF stretchable electrode, as compared with **c,** the corresponding DC conductivity for conventional stretchable electrodes previously reported in the literature. The nGF stretchable electrode shows an extremely broad working range of conductivity with the reverse tendency of the previously reported electrodes. In particular, a very low initial conductivity ($<10^{-4}$ S cm^{-1}), such as in the case of an insulator, makes the development of a zero-standby-power strain sensor feasible.

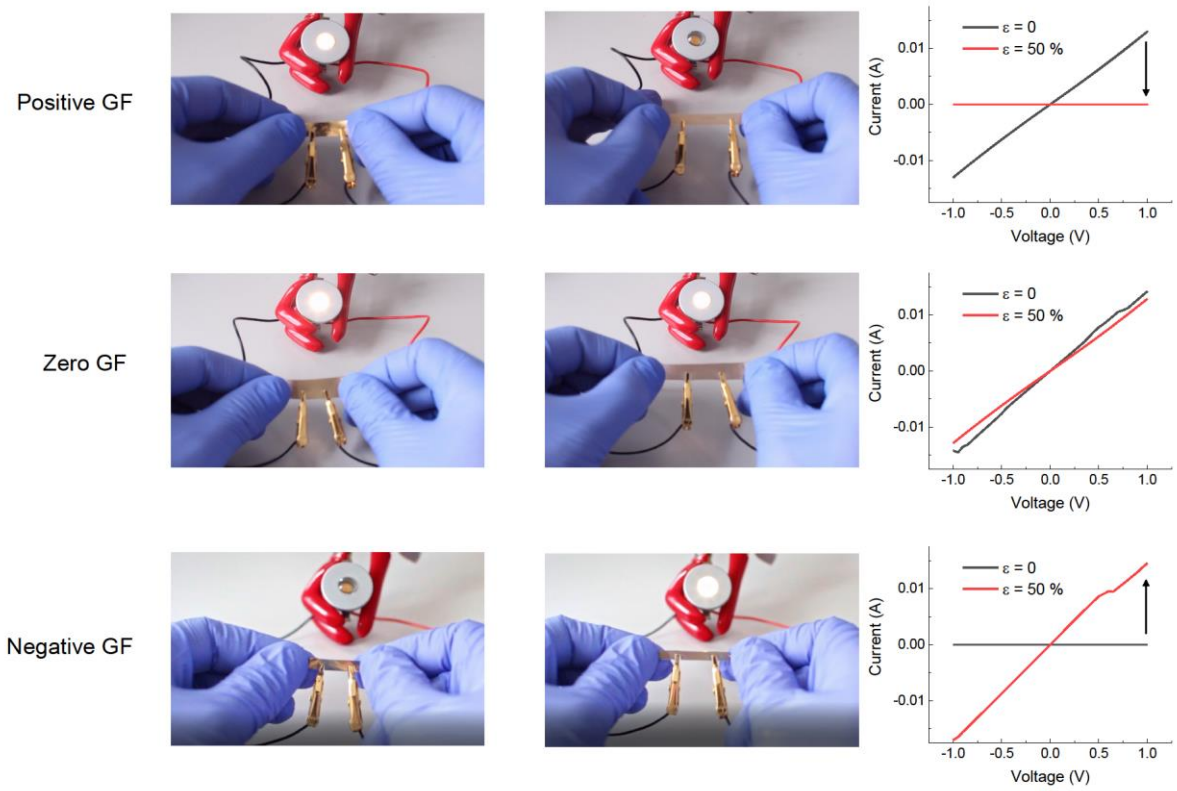

Figure 5. Mechano-gated stretchable switching device. Switching-on test of a light-emitting diode (LED) bulb and the corresponding *I–V* curves for a stretched nGF-stretchable piezoresistor used as stretchable interconnector (left: without stretching; right: with stretching to 50%).The results show a dramatic transition from insulator-like to metal-like conduction under stretching (bottom). The design also shows the other GF electrode modes (pGF: top, zGF: middle) induced through precise control of the experimental parameters.

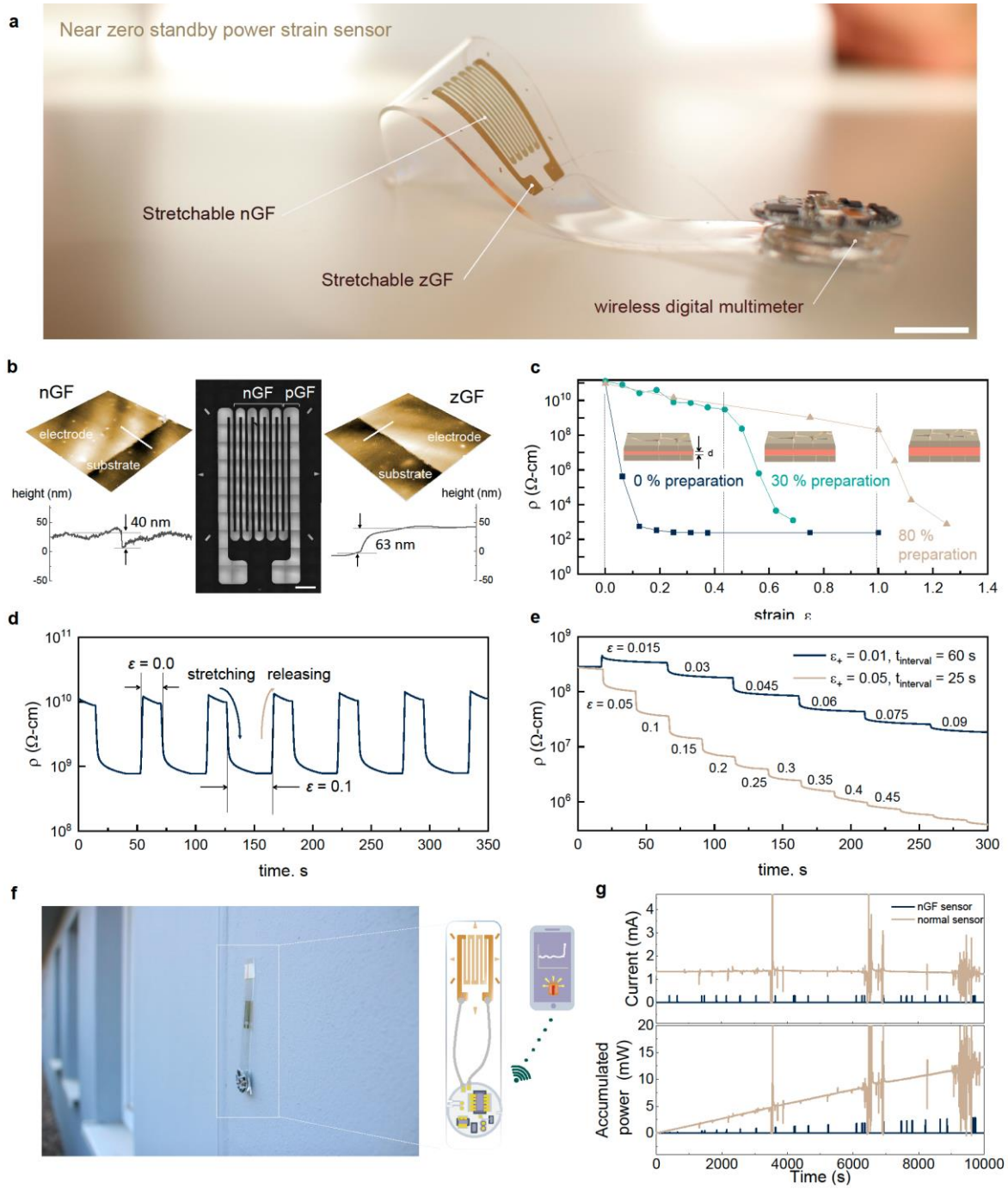

Figure 6. Demonstration of nGF piezoresistive elastomer for standby zero-power strain sensor. a,**b,** As-fabricated zero-standby-power strain sensor utilizing an nGF electrode array. The active sensing grid comprises an nGF electrode (with thickness combination "C" in Fig. 2a), whereas the pad and connector are realized by a zGF electrode (combination "B" in Fig. 2a). Scale bar denotes 1 cm and 1 mm in Fig. 6a and Fig. 6b, respectively. **c-e**, Strain sensing performance. **c,** Modulation of threshold strain of the transition by controlling the initial thickness of the tunneling barrier (Supplementary Information S4). **d,** Reversible strain

sensor performance in the ε = 0.1 strain regime. **e,** Resistivity response to stepwise increments of strain with different applied strain and time intervals, showing accurate and reliable strain-sensor performance. **f, g** Possible single strain gauge circuit with an nGF electrode, realizing near-zero-power standby monitoring. **f**, A digital image of the developed strain sensor integrated onto infrastructure. **g**, Measured drift current and accumulated power of an nGF strain sensor versus a normal strain gauge, plotted as a function of the standby monitoring time.

References

1. Byun, S. H. *et al.* Mechanically transformative electronics, sensors, and implantable devices. *Sci. Adv.* **5**, (2019).
2. Kim, D. H., Ghaffari, R., Lu, N. & Rogers, J. A. Flexible and stretchable electronics for biointegrated devices. *Annu. Rev. Biomed. Eng.* **14**, 113–128 (2012).
3. Mannsfeld, S. C. B. *et al.* Highly sensitive flexible pressure sensors with microstructured rubber dielectric layers. *Nat. Mater.* **9**, 859–864 (2010).
4. Wang, C. *et al.* User-interactive electronic skin for instantaneous pressure visualization. *Nat. Mater.* **12**, 899–904 (2013).
5. Kim, K. K. *et al.* Highly Sensitive and Stretchable Multidimensional Strain Sensor with Prestrained Anisotropic Metal Nanowire Percolation Networks. *Nano Lett.* **15**, 5240–5247 (2015).
6. Trung, T. Q. & Lee, N. E. Flexible and Stretchable Physical Sensor Integrated Platforms for Wearable Human-Activity Monitoringand Personal Healthcare. *Adv. Mater.* **28**, 4338–4372 (2016).
7. Lee, S. *et al.* A transparent bending-insensitive pressure sensor. *Nat. Nanotechnol.* **11**, 472–478 (2016).
8. Rich, S. I., Wood, R. J. & Majidi, C. Untethered soft robotics. *Nat. Electron.* **1**, 102–112 (2018).
9. Larson, C. *et al.* Highly stretchable electroluminescent skin for optical signaling and tactile sensing. *Science (80-.).* **351**, 1071–1074 (2016).
10. Duan, L., D'hooge, D. R. & Cardon, L. Recent progress on flexible and stretchable piezoresistive strain sensors: From design to application. *Prog. Mater. Sci.* 100617 (2020) doi:10.1016/j.pmatsci.2019.100617.
11. Gullapalli, H. *et al.* Flexible piezoelectric zno-paper nanocomposite strain sensor. *Small* **6**, 1641–1646 (2010).
12. Fiorillo, A. S., Critello, C. D. & Pullano, A. S. Theory, technology and applications of piezoresistive sensors: A review. *Sensors Actuators, A Phys.* **281**, 156–175 (2018).
13. Lugstein, A., Steinmair, M., Steiger, A., Kosina, H. & Bertagnolli, E. Anomalous piezoresistance effect in ultrastrained silicon nanowires. *Nano Lett.* **10**, 3204–3208 (2010).
14. Tsai, M. Y. *et al.* Flexible MoS2 Field-Effect Transistors for Gate-Tunable Piezoresistive Strain Sensors. *ACS Appl. Mater. Interfaces* **7**, 12850–12855 (2015).
15. Manzeli, S., Allain, A., Ghadimi, A. & Kis, A. Piezoresistivity and Strain-induced Band Gap Tuning in Atomically Thin MoS2. *Nano Lett.* **15**, 5330–5335 (2015).
16. Biccai, S. *et al.* Negative Gauge Factor Piezoresistive Composites Based on Polymers Filled with MoS2 Nanosheets. *ACS Nano* **13**, 6845–6855 (2019).
17. Yang, Z. *et al.* Graphene Textile Strain Sensor with Negative Resistance Variation for

Human Motion Detection. *ACS Nano* **12**, 9134–9141 (2018).

18. Zhao, K., Niu, W. & Zhang, S. Highly stretchable, breathable and negative resistance variation textile strain sensor with excellent mechanical stability for wearable electronics. *J. Mater. Sci.* **55**, 2439–2453 (2020).

19. Sekitani, T. *et al.* A rubberlike stretchable active matrix using elastic conductors. *Science (80-.).* **321**, 1468–1472 (2008).

20. Chun, K. Y. *et al.* Highly conductive, printable and stretchable composite films of carbon nanotubes and silver. *Nat. Nanotechnol.* **5**, 853–857 (2010).

21. Park, M. *et al.* Highly stretchable electric circuits from a composite material of silver nanoparticles and elastomeric fibres. *Nat. Nanotechnol.* **7**, 803–809 (2012).

22. Matsuhisa, N. *et al.* Printable elastic conductors by in situ formation of silver nanoparticles from silver flakes. *Nat. Mater.* **16**, 834–840 (2017).

23. Matsuhisa, N. *et al.* Printable elastic conductors with a high conductivity for electronic textile applications. *Nat. Commun.* **6**, 1–11 (2015).

24. Stoyanov, H., Kollosche, M., Risse, S., Waché, R. & Kofod, G. Soft conductive elastomer materials for stretchable electronics and voltage controlled artificial muscles. *Adv. Mater.* **25**, 578–583 (2013).

25. Kim, Y. *et al.* Stretchable nanoparticle conductors with self-organized conductive pathways. *Nature* **500**, 59–63 (2013).

26. Simmons, J. G. Generalized Formula for the Electric Tunnel Effect between Similar Electrodes Separated by a Thin Insulating Film. *J. Appl. Phys.* **34**, 1793–1803 (1963).

27. Matthews, N., Hagmann, M. J. & Mayer, A. Comment: ‘generalized formula for the electric tunnel effect between similar electrodes separated by a thin insulating film’ [J. Appl. Phys. 34, 1793 (1963)]. *J. Appl. Phys.* **123**, 1–2 (2018).

Methods

PDMS preparation

The PDMS substrate was prepared by mixing PDMS prepolymer (Sylgard 184, Dow Corning) with a curing agent (Sylgard 184, Dow Corning) at a 10:1 weight ratio. The resultant mixture was poured into a flat Petri dish, maintained at room temperature for 8 h, and then thermally cured at 35 °C for 12 h. The cured PDMS slab with 1.0 mm thickness was used as a substrate and as a reservoir for the diffusion of PDMS to form an intermediate PDMS layer, with no further treatment.

Au thin-film deposition

The PDMS substrate was mounted onto a sample holder for PVD (chamber: Hex, Korvus Technology) and a Au thin film was deposited by thermal evaporation. The deposition rate was 0.3 Å s^{-1} with the deposition chamber evacuated to a pressure less than 6.2×10^{-6} mbar. The thickness was monitored in situ by quartz crystal microbalance.

Soft tunneling barrier formation

After a Au thin film was deposited onto the PDMS substrate, the sample was stretched to 80% strain to induce cracks in the Au thin film. The sample was kept under a reduced pressure of 6.0×10^{-6} mbar for 8 h afterwards.

Electrical characterization measurement

A Keithley 2612B sourcemeter was used for the DC electrical conductivity and resistivity measurements of all samples. The probe station (TS50, MPI AST) was equipped with a four-point probe tip of tungsten. The specimens for the resistivity and conductivity calculations

were defined within an area of 1 cm × 1 mm, and the leads of the probe tip were directly connected to the pristine surface of samples. The tips were attached and detached onto stretched sample surfaces to maintain the distance between each tip. For the real-time strain sensor, measurement of a silicone conductor (RTV-SNC-015, Euro Technology) was used to sustain the electrical contact during the strain-release cycle.

Characterizations

All of the atomic force microscopy images were obtained with an MFP-3D atomic force microscope (Asylum Research, USA). For the cross-sectional TEM images, the nGF sample was prepared as lamellar thin slices by focused ion beam (FIB) (JIB-4601F, JEOL); TEM analysis was then conducted (JEM-ARM 200F, JEOL). For the cross-sectional SEM analysis (NEON40, ZEISS), various thicknesses of nGF samples were cross-sectioned by FIB. THz-TDS measurements were performed using a homemade setup based on a Ti:sapphire femtosecond laser amplifier (Coherent RegA 9000), a photoconductive GaAs THz emitter, and a ZnTe electro-optic detector. The covered spectral range was 0.3 to 2.7 THz. For a series of confocal microscopic images under applied strain in situ, the nGF samples were mounted onto a homemade motorized linear stage (L505, PI) and the stage was placed under a Nanofocus™ confocal microscope. Water contact angles on the nGF sample surfaces were measured using DataPhysics OCA35L. Thin PDMS layer thicknesses were obtained by modeling ellipsometric data (M2000-UI, J.A. Woollam Co. Inc., USA) using a fixed-refractive-index dispersion of $n(\lambda) = 1.38 + 0.01/\lambda^2$ [λ in μm], obtained for a mm-thick PDMS film supported on a Si substrate.

Fabrication of zero-power wireless strain-sensor

The patterned electrode was deposited onto a long stripe of PDMS substrate by stencil mask, and the wireless digital multimeter (Pokitmeter™) was integrated onto the bottom of

the PDMS substrate and electrically contacted to the electrode pattern of the nGF stretchable strain sensor by conductive silicone rubber (RTV-SNC-015, Euro Technology). The wireless real-time monitoring was conducted by Bluetooth® communication via a commercial smart mobile device (iPhone 6s, Apple).

Contribution

S. C conceived and designed the work and conducted the electrical characterization of the device under the supervision of A.F. I.F. and A.P. conducted the THz-tds experiments and related data analysis and interpretation. A.P. modeled and interpreted the strain-dependent conductance based on Simmons' tunneling equation. E.B. carried out the ellipsometry measurement and conducted related data analysis. W.J.C. calculated the theoretical thickness change of the soft barrier by FEM. S. C W. J. C. and A.P. wrote the manuscript. P.U., M.S. and A.P. edited the manuscript. All authors discussed the results.

Acknowledgement

S. Chae was fully supported by an Alexander von Humboldt postdoc fellowship. The authors thank Anik Kumar Ghosh, Takuya Tsuda and Dr. Petr Formanek at IPF for assistance with the fabrication and electrical characterization of the nGF piezoresistive elastomer.

Figures

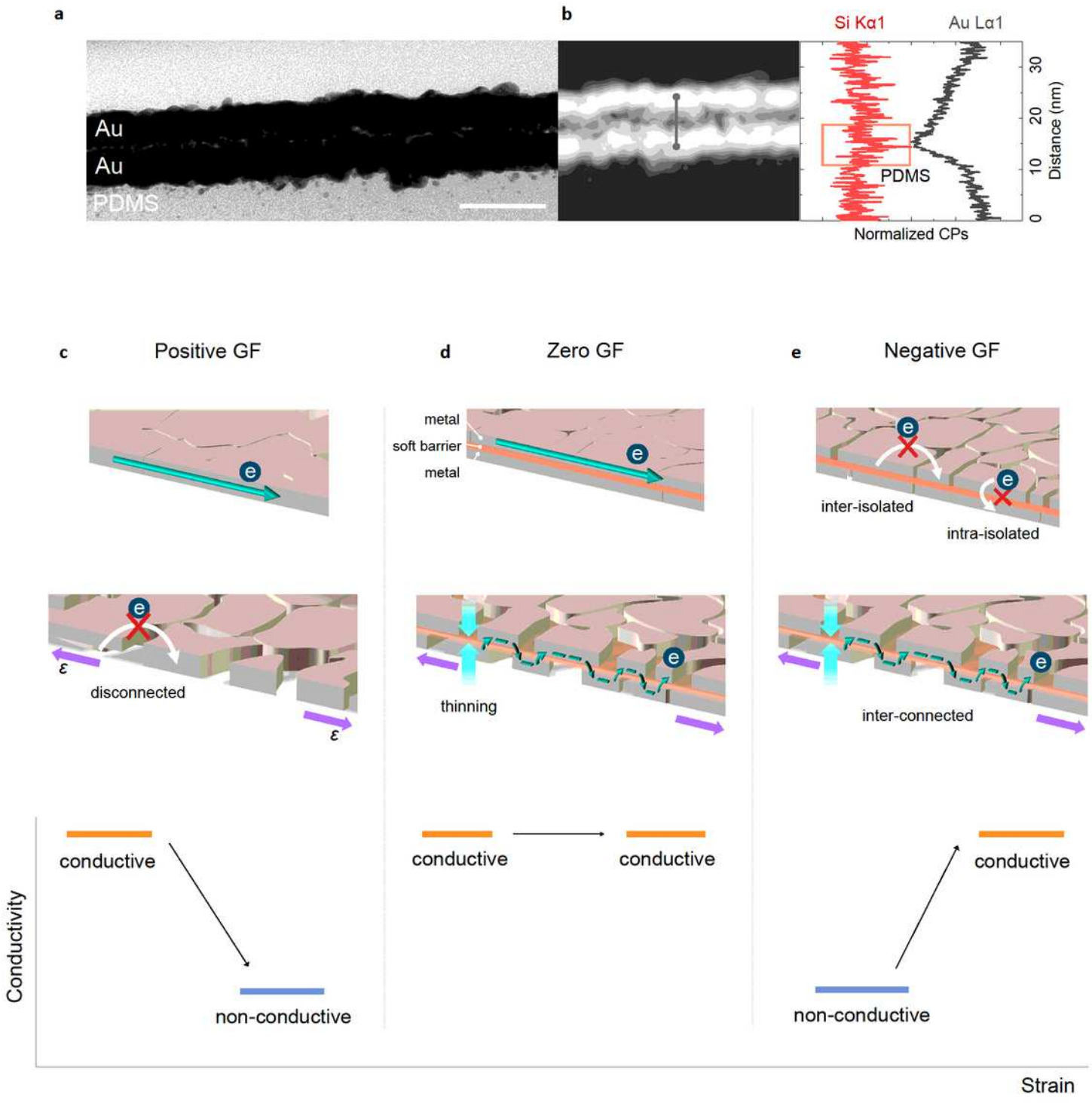

Figure 1

Sandwiched bilayer metal thin film with a soft barrier layer for all types of piezoresistive stretchable electrodes. a, nGF stretchable piezoresistive device with a bimetal layer (each 20–30 nm thick) and thin soft insulator barrier layer (~12 nm thick); scale bar, 100 nm. b, Scanning TEM image of the device with

line profile of the energy-dispersive X-ray spectra of Si and Au atoms for identifying the soft barrier layer (e.g., PDMS) sandwiched in the metal thin-film bilayer (e.g., Au). c,d,e, With precise control of the deposition thickness of the bimetal thin film (e.g., percolation engineering) and quantum-scale thinning of the soft barrier layer upon stretching, the designed structure shows all three modes of GF (c, pGF; d, zGF; e, nGF). In particular, for the nGF property, an extremely high on/off electrical conductivity ratio was obtained over a wide range of working strains.

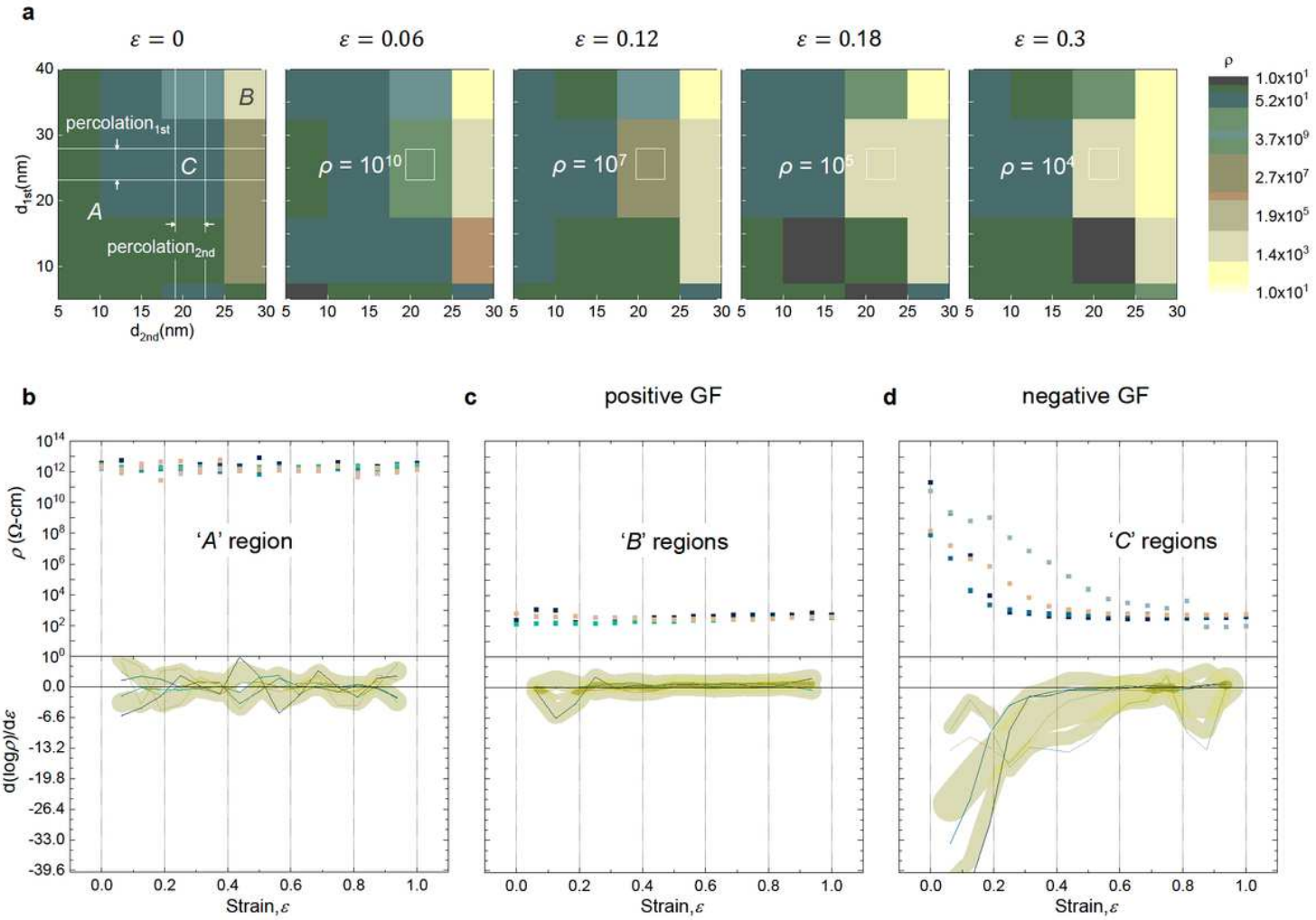

Figure 2

Thickness effect of the metal layer on nGF behavior. a, The nGF behavior is dependent on the thickness of the bimetal layer. For different combinations of the two layer thicknesses (vertical axis: first layer; horizontal axis: second layer), the change tendency of resistivity in the bilayer electrode with various strains (ε = 0, 0.06, 0.12, 0.18, 0.3) was classified as constant insulator-like (“A” combination), constant metal-like conduction (“B” combination), and transition from insulator-like to a metal-like conduction, nGF (“C” combination), where the percolation thickness of each metal layer is the criterion for determining the classification (see Supplementary Fig. 5). b,c,d, The resistivity change of respective regions in the full range of applied strain (ε = 0 – 1) and the corresponding rate of change for the “A” combination (b), “B”

combination (c), and “C” combination (d). A stretchable device satisfying combination “C” shows only the dramatic transition in resistivity under applied strain, i.e., high nGF performance.

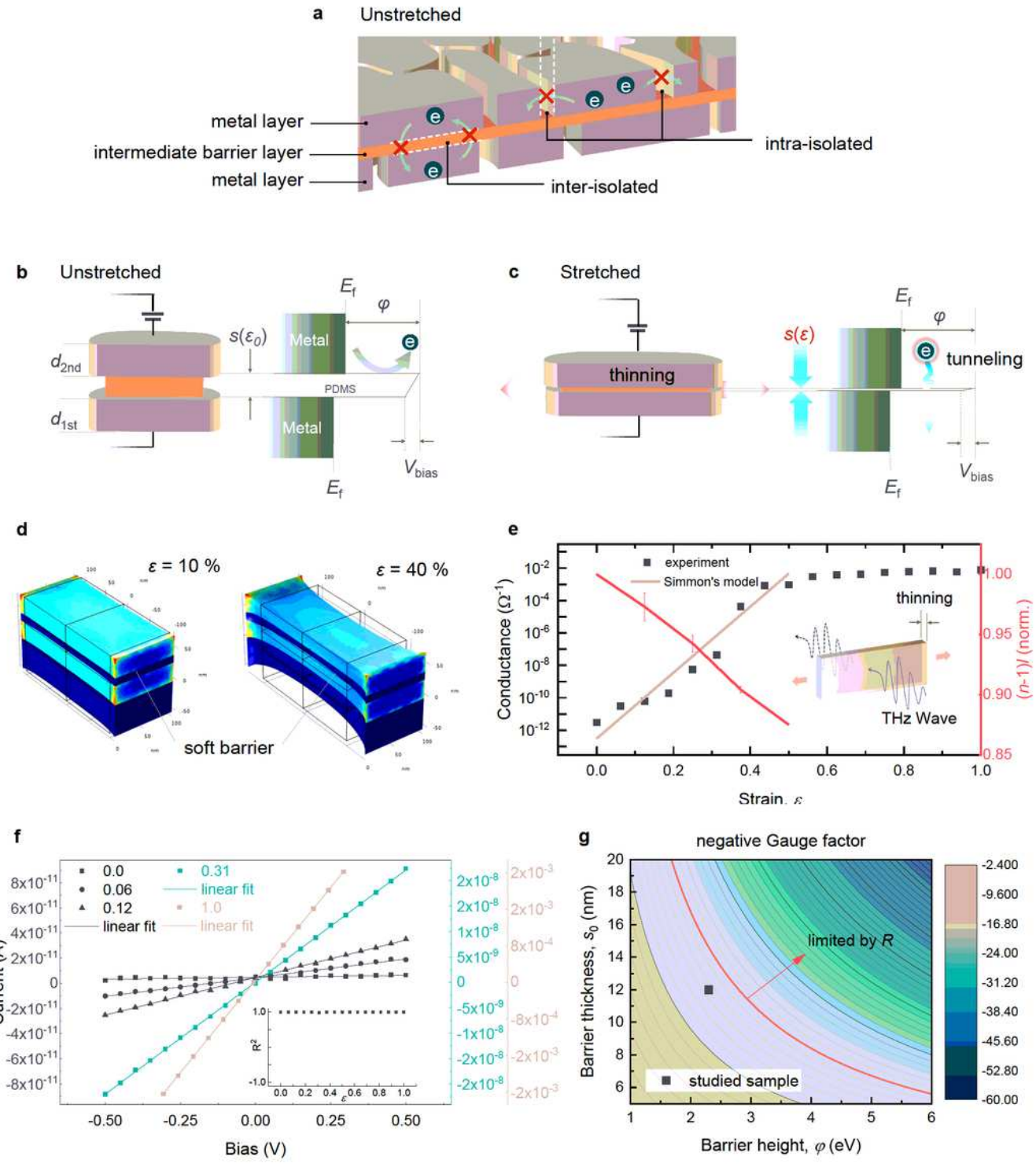

Figure 3

Working principle of the nGF piezoresistive device: tunneling current caused by thinning of the soft barrier layer. a, Schematic of the nGF piezoresistive device in its initial state (without stretching), where two metal layers are electrically not only intra-isolated via controlled percolation but also interisolated by an

inserted thin soft intermediate insulating layer. b,c, Energy-level diagrams of an nGF stretchable electrode in the unstretched (b) and stretched (c) states, where electrons transport through the thinned barrier layer caused by stretching (sε), whereas no electron transport occurs because of the sufficient thickness (sε0) with a high barrier height (φ) without stretching. d, Theoretical thinning of the soft barrier layer simulated by the finite element method (Supplementary Fig. 7). e, Strain-dependent conductance with experimentally measured thinning of the soft barrier layer, as measured by THz-TDS (red line). Measured conductance of an nGF stretchable electrode sample (black dots) and the calculation according to low-voltage limited Simmons' tunneling equation, Eq. (1) (brown line). f, I–V curves of an nGF stretchable device at different applied strains; all of the curves show linear behavior independent of the applied strain. Note that the current scales differ for different applied strains (inset: R2 of the linear fit in the strain range from 0.0 to 1.0). g, Expected nGF as a function of the variation in the potential barrier height and the initial thickness of the soft barrier layer. Solid black squares (e.g., nGF = −14.8) indicate the nGF value for the sample studied in this work. Note that, beyond the red boundary line, the nGF value could be limited in practical applications because of excessively high resistance. Each line corresponds to an nGF level from −5 to −50 with a step of 10.

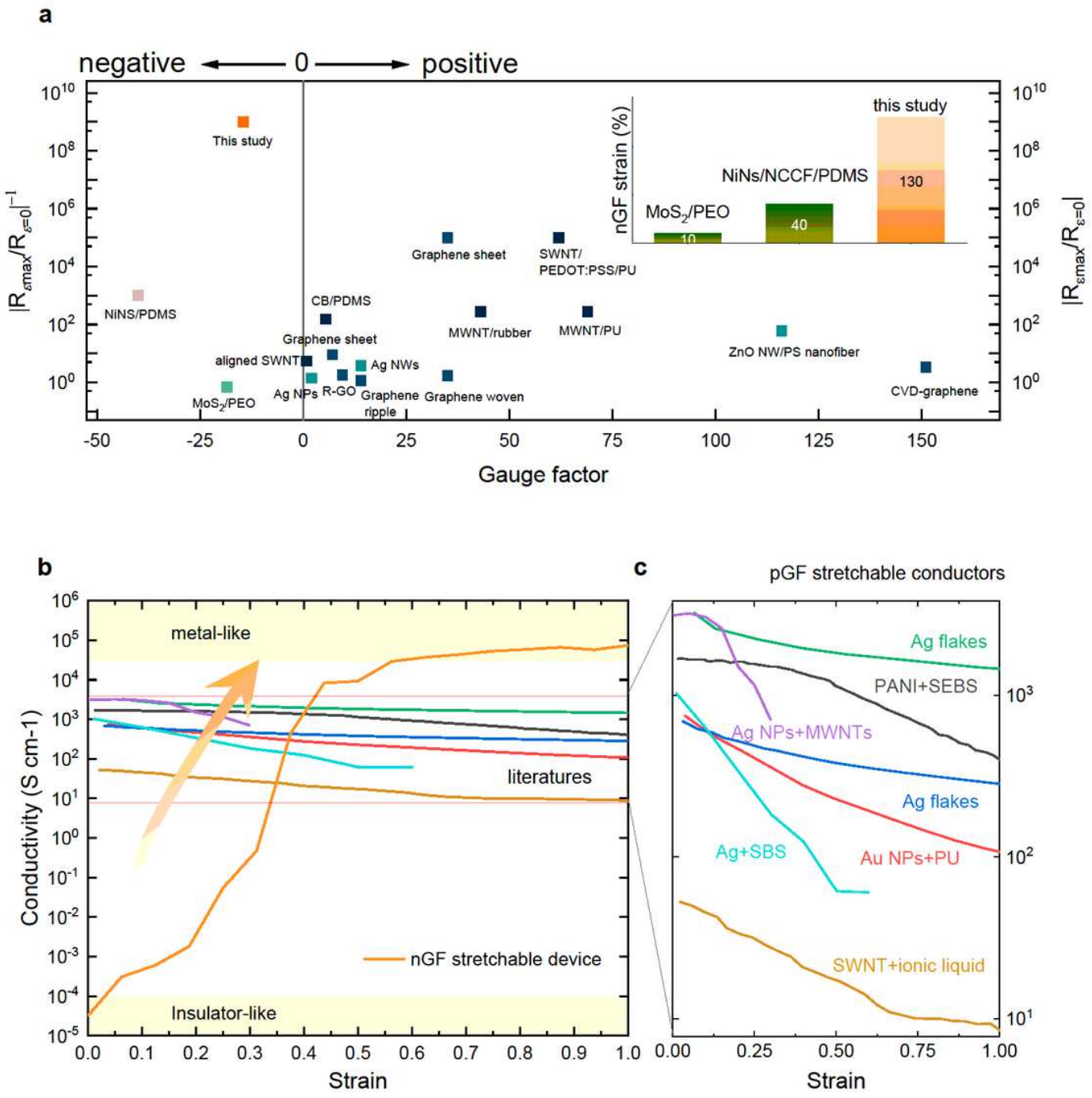

Figure 4

High performance of the nGF piezoresistive stretchable structure. a, The performance of the bilayer metal nGF stretchable electrode is compared with that of state-of-the-art stretchable piezoresistive materials. The maximum nGF strain range (to 130%) of the bilayer metal stretchable electrode represents the best-available stretchability among the developed negative piezoresistive materials (inset). b, Measured DC conductivity with respect to applied strain of the nGF stretchable electrode, as compared with c, the corresponding DC conductivity for conventional stretchable electrodes previously reported in the literature. The nGF stretchable electrode shows an extremely broad working range of conductivity with the

reverse tendency of the previously reported electrodes. In particular, a very low initial conductivity (<10−4 S cm−1), such as in the case of an insulator, makes the development of a zero-standby-power strain sensor feasible.

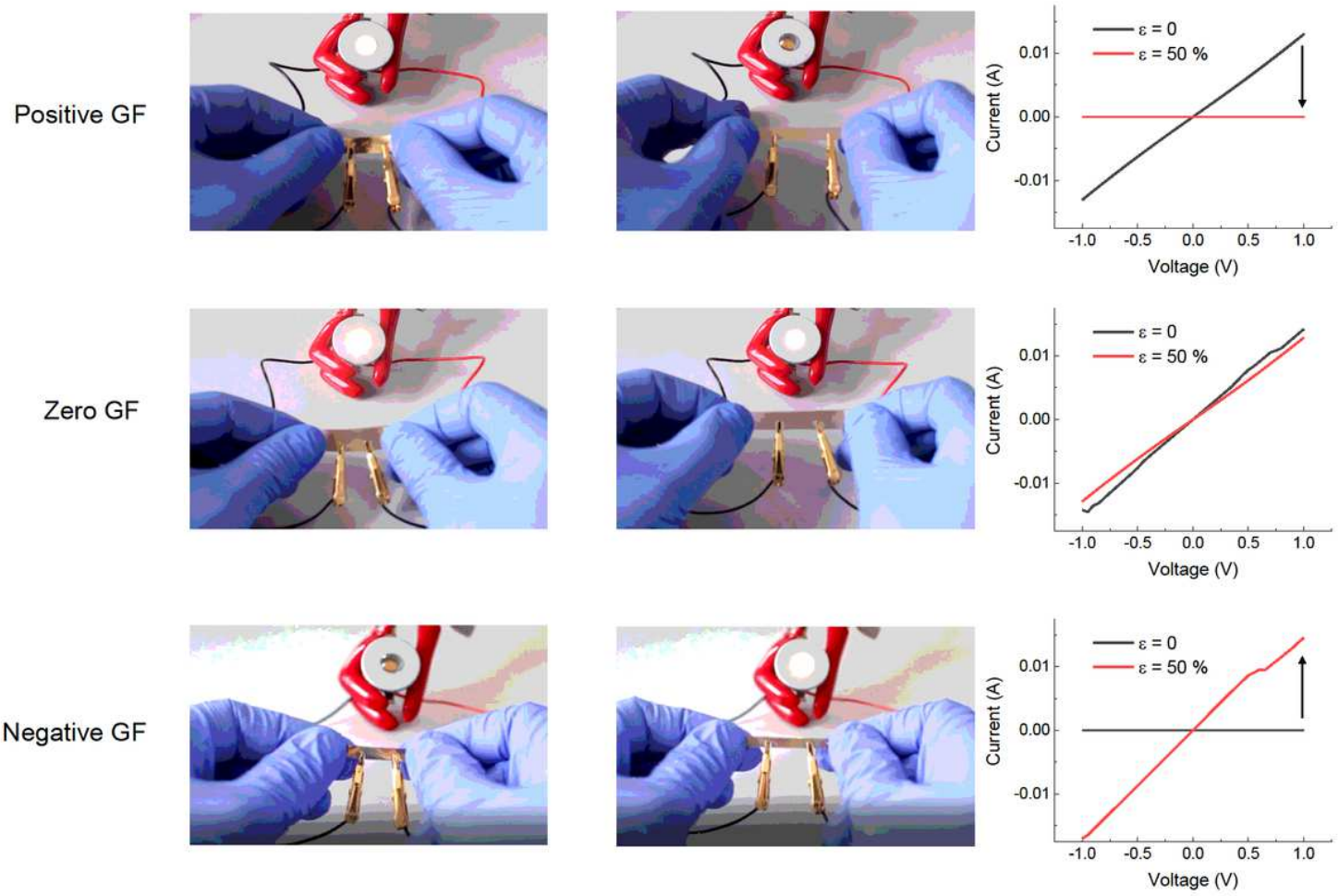

Figure 5

Mechano-gated stretchable switching device. Switching-on test of a light-emitting diode (LED) bulb and the corresponding I–V curves for a stretched nGF-stretchable piezoresistor used as stretchable interconnector (left: without stretching; right: with stretching to 50%).The results show a dramatic transition from insulator-like to metal-like conduction under stretching (bottom). The design also shows the other GF electrode modes (pGF: top, zGF: middle) induced through precise control of the experimental parameters.

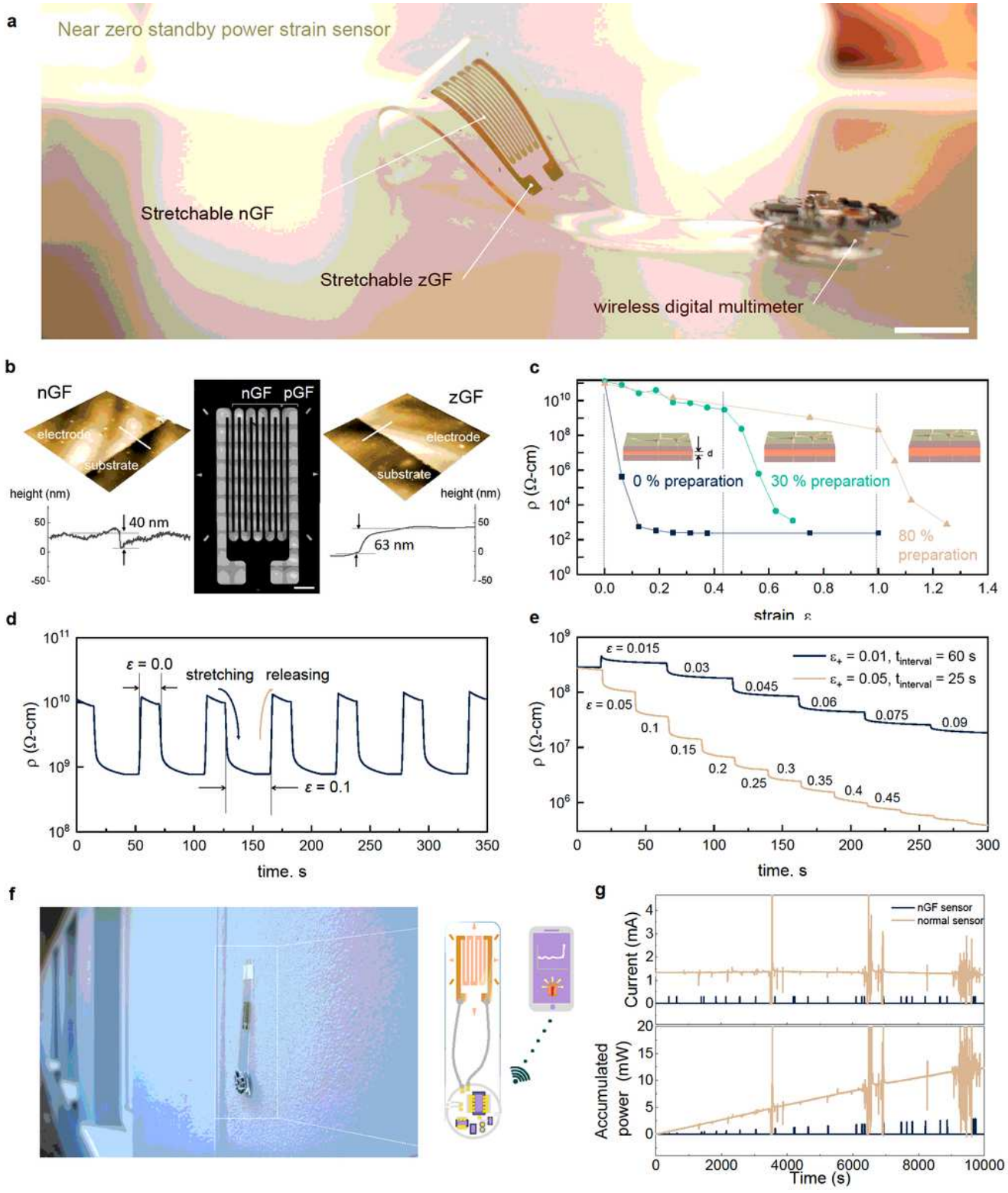

Figure 6

Demonstration of nGF piezoresistive elastomer for standby zero-power strain sensor. a,b, As-fabricated zero-standby-power strain sensor utilizing an nGF electrode array. The active sensing grid comprises an nGF electrode (with thickness combination “C” in Fig. 2a), whereas the pad and connector are realized by a zGF electrode (combination “B” in Fig. 2a). Scale bar denotes 1 cm and 1 mm in Fig. 6a and Fig. 6b, respectively. c-e, Strain sensing performance. c, Modulation of threshold strain of the transition by

controlling the initial thickness of the tunneling barrier (Supplementary Information S4). d, Reversible strain sensor performance in the ε = 0.1 strain regime. e, Resistivity response to stepwise increments of strain with different applied strain and time intervals, showing accurate and reliable strain-sensor performance. f, g Possible single strain gauge circuit with an nGF electrode, realizing near-zero-power standby monitoring. f, A digital image of the developed strain sensor integrated onto infrastructure. g, Measured drift current and accumulated power of an nGF strain sensor versus a normal strain gauge, plotted as a function of the standby monitoring time.

Supplementary Files

This is a list of supplementary files associated with this preprint. Click to download.

- SupplementaryMovie1.mp4
- SupplementaryInformationnGF.docx